VPS VIBRATIONS IN PHYSICAL SYSTEMS

DOI: 10.21008/j.0860-6897.2021.2.09
Vibrations in Physical Systems, 32(2):2021209, 2021

Assessment of the Role of Structural Nonlinearity in Galloping Energy Harvesters

Filip SARBINOWSKI[1], Roman STAROSTA[1]

Corresponding author: Filip SARBINOWSKI, email: filip.j.sarbinowski@doctorate.put.poznan.pl

[1] Poznan University of Technology, Institute of Applied Mechanics, Jana Pawła II 24, 60-956 Poznań, Poland

Abstract The study compares different variants of aeroelastic energy harvesters due to the power they generate. For this purpose, models of devices with different stiffness characteristics were prepared: linear, nonlinear, with combined stiffness and bistable. Then, using the authorial procedure, analytical expressions that describe the power of each system were determined and the influence of individual parameters on this quantity was examined. By way of optimization, the system parameters have been selected in such a way that, regardless of the flow velocity, each of them generates the maximum possible power. Based on the results obtained in this way, the advisability of using a device with combined stiffness and bistable characteristics was rejected. Moreover, it was pointed out that the linear system would provide greater efficiency for lower flow velocities.

Keywords: energy harvesting, aeroelasticity, self-induced vibration, galloping

1. Introduction

Along with the development of industry and the related climate changes in the past several decades, the importance of developing renewable energy sources has evolved from a technological curiosity and a way to reduce energy costs to one of the most important goals of humanity. The attempts to develop an alternative – cheaper and more efficient – devices recovering energy from the environment are a natural reaction to this state of affairs. An example of such a device is the galloping energy harvester (GEH), which recovers energy from vibrations induced by the flow. this phenomenon was first described in [1], and then significantly expanded in [2]. According to these works, we consider a body with one degree of freedom (translation parallel to axis Z), mounted on the lumped element system, subjected to flow parallel to the X-axis (see Figure 1). The dynamics of the system is described by the equation:

$$m\ddot{z}(t) + c\dot{z}(t) + \frac{\partial E_p}{\partial z(t)} = F_z(\alpha) = \frac{1}{2}\, h\rho U^2 C_z(\alpha), \tag{1}$$

where: m – mass of the body [kg], c –damping coefficient [kg/s], k – stiffness coefficient [N/m], $z(t)$ – displacement in the Z direction [m], $\dot{()}$ and $\ddot{()}$ – first and second divertive with respect to time, $C_z(\alpha)$ – coefficient of aerodynamic force acting in the Z direction at α angular orientation of the body, E_p – potential energy [J], F_Z – aerodynamic force component acting in the Z direction [N], h – characteristic length of the body [m], ρ – fluid density [kg/m^2], U – flow velocity [m/s]. In Figure 1 it can be seen that:

$$F_z(\alpha) = -F_L\cos(\alpha) - F_D\sin(\alpha) \approx -(F_L + F_D\,\alpha), \tag{2}$$

and after expanding in Taylor's series:

$$F_L + F_D\alpha = F_L + \left(\frac{dF_L}{d\alpha} + F_D\right)\alpha + \left(\frac{1}{2}\frac{d^2F_L}{d\alpha^2} + \frac{dF_D}{d\alpha}\right)\alpha^2 + \frac{1}{6}\left(\frac{d^3F_L}{d\alpha^3} + 3\frac{d^2F_D}{d\alpha^2}\right)\alpha^3 + \mathcal{O}(\alpha^4), \tag{3}$$

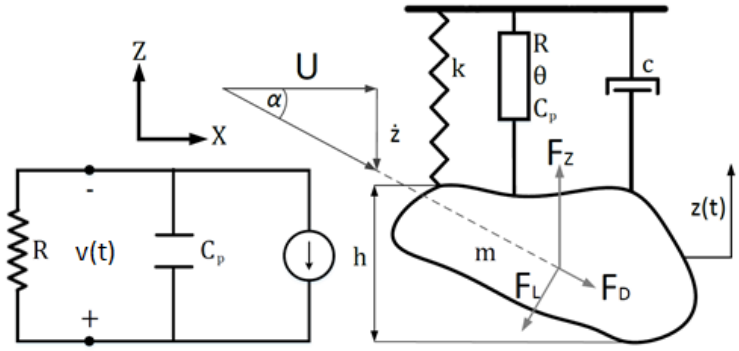

Fig. 1. Physical model of the aeroelastic energy harvester. F_L – lift force, F_D – drag force.

Due to the fact that the elastic force of the system is linear, constant force component F_L does not affect the dynamics of the device, therefore, it will be neglected in further considerations. The only factors affecting the aerodynamic force depending on the α angle are aerodynamic coefficients, hence:

$$C_z(\alpha) = \left(\frac{dC_L}{d\alpha} + C_D\right)\alpha + \left(\frac{1}{2}\frac{d^2C_L}{d\alpha^2} + \frac{dC_D}{d\alpha}\right)\alpha^2 + \frac{1}{6}\left(\frac{d^3C_L}{d\alpha^3} + 3\frac{d^2C_D}{d\alpha^2}\right)\alpha^3 + \mathcal{O}(\alpha^4). \tag{4}$$

Research made in [2, 3] confirms above derivation of the $C_z(\alpha)$ function, and [4] shows that third-order approximation is sufficient for energy harvesting purposes. We also assume that the flowed body has a symmetry axis in the direction normal to the flow. In this case, the even coefficients a_n will be equal to zero:

$$C_z(\alpha) \approx a_1\,\alpha + a_3\,\alpha^3, \tag{5}$$

where $a_1 = \left(\frac{dC_L}{d\alpha} + C_D\right)$ and $a_3 = \frac{1}{6}\left(\frac{d^3C_L}{d\alpha^3} + 3\frac{d^2C_D}{d\alpha^2}\right)$. The mathematical model of the phenomenon thus takes the form:

$$m\ddot{z}(t) + c\dot{z}(t) + \frac{\partial V}{\partial z(t)} = -\frac{1}{2}\rho U^2 h\left(a_1\frac{\dot{z}(t)}{U} + a_3\left(\frac{\dot{z}(t)}{U}\right)^3\right). \tag{6}$$

The device must be equipped with a converter that will convert mechanical energy into electrical energy. For this purpose, among others, electrostatic transducers that may be the cheapest solution for large scale production [5, 6]. Electromagnetic transducers are characterized by large size and high cost [7, 8], but their unquestionable advantage is high efficiency. The multitude of possible transducer designs of this type increases their versatility, allowing their use in both small devices [9] and massive hydro or wind power plants. Prototypes, however, most often are consist of piezoelectric transducers [10–12], which is justified by great simplicity in their implementation while maintaining high efficiency. It will also be used in this work. The mathematical model of piezoelectric vibration energy harvester (PVEH) takes the form [13]:

$$m\,\ddot{z}(t) + c\,\dot{z}(t) + \frac{\partial E_p}{\partial z(t)} + \theta\,v(t) = -\frac{1}{2}\rho U^2 h\left(a_1\frac{\dot{z}(t)}{U} + a_3\left(\frac{\dot{z}(t)}{U}\right)^3\right), \tag{7}$$

$$C_p\,\dot{v}(t) + \frac{v(t)}{R} - \theta\,\dot{z}(t) = 0, \tag{8}$$

where: $v(t)$ – generated voltage [V], θ – electromechanical coupling [N/V], R – circuit resistance [Ω], C_p– circuit equivalent capacity [F]. Mathematical model (eqs. 7, 8) can be rewritten in dimensionless form by introducing dimensionless parameters:

$$\ddot{w}(\tau) + 2\zeta\,\dot{w}(\tau) + \frac{\partial \Psi}{\partial \eta(\tau)} + \kappa\,n(\tau) = -\left(a_1\,\bar{\rho}\,\bar{U}\,\dot{w}(\tau) + a_3\,\bar{\rho}\frac{\dot{w}(\tau)^3}{\bar{U}^3}\right), \tag{9}$$

$$\dot{n}(\tau) + \frac{n(\tau)}{r} - \dot{w}(\tau) = 0, \tag{10}$$

where: $w(\tau) = \frac{z(t)}{h}, n(\tau) = \frac{v(t)}{\theta\, Cp} h, \zeta = \frac{c}{2m\,\omega_n}, \Psi = \frac{E_p}{k\,h^2}, \kappa = \frac{\theta^2}{Cp\, m\, {\omega_n}^2}, \bar{\rho} = \frac{h^2\,\rho}{2m}, r = C_p\,\omega_n\,R, \bar{U} = \frac{U}{h\,\omega_n}, \tau = \omega_n\, t.$

In recent years the influence of individual parameters of the system on its efficiency has been intensively studied. In [14] elliptical cross-sections with different ratios between the length of the semi-minor axis and the semi-major axis were examined. A substantial set of aerodynamic coefficients of various typical sections is included in [15]. The maximum efficiency of PVEH depending on the shape of the flowing body was analyzed in [16]. The work [17] is devoted to the analysis of the impact of trapezoid arm inclination on its aerodynamic coefficients.

Another factor strongly affecting the performance of PVEH is its mechanical structure. The typical one degree of freedom beam devices [18, 19] seems to give way in this respect to a more complex multi-degree of freedom systems [20 - 22]. It is worth noting that devices exhibit also torsional vibrations should not be modeled using Den Hartog's hypothesis – for torsional vibrations the quasi stationarity condition is never satisfied. The nonstationary flow model was used, among others in works [23, 24]. One can also indicate many variants of the device with nonlinear mechanical properties [25, 26, 14], but – according to the best knowledge of the authors – no work has been done so far to compare and evaluate them.

In this paper, we compare the electric powers generated by various PVEH variants: linear, with hardening stiffness characteristics, softening stiffness characteristics, a family of systems with a freeplay and a bistable system. It should be emphasized that, depending on the structure of the device, the value of a given parameter will affect the performance of the device in different ways. Moreover, the potential energy of individual systems is characterized by different parameters, therefore comparing variants for an arbitrarily selected, universal set of parameters would be inappropriate, even if in some cases it would be possible. The comparison itself will be preceded by the optimization of each system, i.e. selection of such parameters for which it will generate the maximum possible power.

2. Analytical solution

Electrical power generated by the system depends on the flow velocity, therefore it can be expected that the optimal values of the parameters will also be functions of the flow velocity. These functions can be conveniently obtained by calculating the roots of proper power function derivatives, which is easiest to do with an analytical expression describing power. In the most general terms dimensionless power $\bar{P}$ of the systems is given by the formula:

$$\bar{P} = \frac{P}{m h^2 {\omega_n}^3} = \frac{{A_v}^2 (R)^{-1}}{m\, h^2\, {\omega_n}^3} = \frac{\kappa\, {A_n}^2}{2r}, \tag{11}$$

where: P – electrical power [W], A_v – voltage magnitude [V], A_n – dimensionless voltage magnitude. Value of A_n will be determined individually for each device variant based on the analytical solution of the model. Despite the nonlinearity in the system, we assume solutions in the form:

$$w(\tau) = A_w \cos(\Omega\, \tau), \tag{12}$$

$$n(\tau) = A_n \cos(\Omega\, \tau + \varphi), \tag{13}$$

where: A_w – dimensionless amplitude of vibration, $\Omega = \frac{\omega}{\omega_n}$ – dimensionless frequency, A_n – dimensionless voltage magnitude and φ – phase shift are unknown quantities. Functions of φ can be obtained by substituting eq. (12) and eq. (13) to eq. (10):

$$\frac{A_n \cos(\Omega\tau + \varphi)}{r} + A_x \Omega \sin(\Omega\, \tau) - A_n \Omega \sin(\Omega\tau + \varphi) = 0, \tag{14}$$

which for dimensionless time $\tau = 0$ simplifies to the form:

$$\frac{A_n \cos(\varphi)}{r} - A_n \Omega \sin(\varphi) = 0, \tag{15}$$

therefore:

$$\tan(\varphi) = \frac{1}{r\,\Omega}, \tag{16}$$

$$\sin(\varphi) = \frac{1}{\sqrt{(r\Omega)^2 + 1}}, \tag{17}$$

$$\cos(\varphi) = \frac{r\Omega}{\sqrt{(r\Omega)^2 + 1}}. \tag{18}$$

The relation between the dimensionless amplitude of vibration A_x and dimensionless voltage magnitude A_n was determined by substituting eqs. (12, 13) to eq. (10), integrating both sides with respect to dimensionless time in half period boundary $\frac{1}{2}T = \frac{\pi}{\Omega}$ and applying identities (17, 18):

$$\int_0^{\frac{1}{2}T} \dot{n}(\tau)\, d\tau + \int_0^{\frac{1}{2}T} \frac{n(\tau)}{r} d\tau = \int_0^{\frac{1}{2}T} \dot{w}(\tau)\, d\tau. \tag{19}$$

By solving equation (19) we get the expression:

$$A_n = A_w \cos(\varphi) = A_w \frac{r\Omega}{\sqrt{1 + r^2\Omega^2}}. \tag{20}$$

In the expressions (16–18) and (20) no potential energy appears, thus these identities will hold for each device variant. Nevertheless, the functions $\bar{P}$ and hence A_n have to be calculated individually for every type of device. Two missing equations can be obtained by examining the condition of mode shapes orthogonality satisfaction (eqs. (21, 22)). Substitution to these equations eqs. (12, 13), eqs. (17, 18) and eq. 20 and solving them for A_w and Ω provides an approximate analytical solution of the system (9, 10).

$$\int_0^T \left(\ddot{w}(\tau) + 2\zeta\, \dot{w}(\tau) + \frac{\partial \Psi}{\partial w(\tau)} + \kappa\, n(\tau) + a_1\, \bar{\rho}\, \bar{U}\, \dot{w}(\tau) + a_3\, \bar{\rho}\, \frac{\dot{w}(\tau)^3}{\bar{U}} \right) \cos(\Omega\tau)\, d\tau = 0, \tag{21}$$

$$\int_0^T \left(\ddot{w}(\tau) + 2\zeta \dot{w}(\tau) + \frac{\partial \Psi}{\partial w(\tau)} + \kappa\, n(\tau) + a_1\, \bar{\rho}\, \bar{U}\, \dot{w}(\tau) + a_3\, \bar{\rho}\, \frac{\dot{w}(\tau)^3}{\bar{U}} \right) \sin(\Omega\tau)\, d\tau = 0. \tag{22}$$

It should be emphasized that even though the solution will depend on all the parameters present in the model, the optimization considering each of them is pointless according to the purpose of the work. Parameters a_1 and a_3 characterize the geometry of the flowing body, which in each case will be the equal, dimensionless density $\bar{\rho}$ as well as dimensionless flow velocity $\bar{U}$ are not quantities related to the structure, while the optimal value of the damping ratio ζ, regardless of the device variant $\zeta_{opt} = 0$. It follows that the only parameters against which the solution should be optimized are: dimensionless electrical resistance r, electromechanical coupling κ, and quantities that describe the potential energy Ψ.

3. Impact of parameter values on the solution

3.1. Linear system

The physical model of the system is shown in Figure 2a.

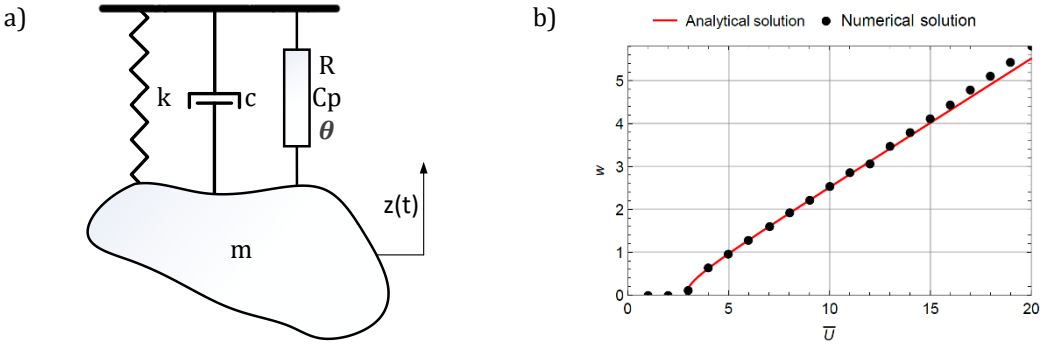

Fig. 2. a) Model of the linear device; b) Variation of vibration amplitude w with flow velocity $\bar{U}$ for the linear model.

The dimensionless restoring force is given by the expression:

$$\frac{\partial \Psi}{\partial w(\tau)} = w(\tau). \tag{23}$$

The solution of eqs. (21, 22) using previously derived expressions leads to obtaining the sought dimensionless values: frequency, vibration amplitude, voltage magnitude and power of the system respectively:

$$\Omega = \sqrt{\frac{1}{2}\left(1 - \frac{1}{r^2} + \kappa + \frac{\sqrt{4r^2 + (1 - r^2 - r^2\kappa)^2}}{r^2}\right)}, \tag{24}$$

$$A_w = 2\sqrt{\frac{r\bar{U} - a_1\bar{\rho}\bar{U}^2 + 2\bar{U}\zeta - a_1\bar{\rho}r^2\bar{U}^2\Omega^2 + 2r^2\bar{U}\zeta\Omega^2}{3a_3\bar{\rho}\Omega^2(1 + r^2\Omega^2)}}, \tag{25}$$

$$A_n = 2\,r\,\Omega\frac{\sqrt{r\bar{U} - a_1\bar{\rho}\bar{U}^2 + 2\bar{U}\zeta - a_1\bar{\rho}\,r^2\bar{U}^2\Omega^2 + 2r^2\bar{U}\zeta\Omega^2}}{\sqrt{3}a_3\bar{\rho}\Omega^2(1 + r^2\Omega^2)}, \tag{26}$$

$$\bar{P} = \frac{4\,r\,\kappa\,\Omega^2\,(r\bar{U} - a_1\bar{\rho}\bar{U}^2 + 2\bar{U}\zeta - a_1\bar{\rho}r^2\bar{U}^2\Omega^2 + 2\,r^2\bar{U}\zeta\Omega^2)}{\left(3a_3\bar{\rho}\Omega^2\,(1 + r^2\Omega^2)\right)^2}. \tag{27}$$

To assess the correctness of assumptions (12, 13), Figure 2b compares the evolution of function (27) and numerical solutions of system (9, 10). This graph also illustrates the fact that the system will not be excited if the flow velocity will not be high enough. This critical velocity is given by the expression:

$$\bar{U}_{cr} = \frac{1 + 4r\zeta + r^2(\kappa + 1) - \sqrt{1 - 2r^2(\kappa - 1) + r^4(\kappa + 1)^2}}{2a_1\bar{\rho}r}. \tag{28}$$

Since no characteristic parameter of the structure appears in the expression for dimensionless potential energy (eq. 21), the only parameters whose impact on power should be examined are dimensionless resistance r and dimensionless electromechanical coupling κ. Graphs of power dependence on these parameters for different flow velocities are shown in Figure 3a and Figure 4a respectively.

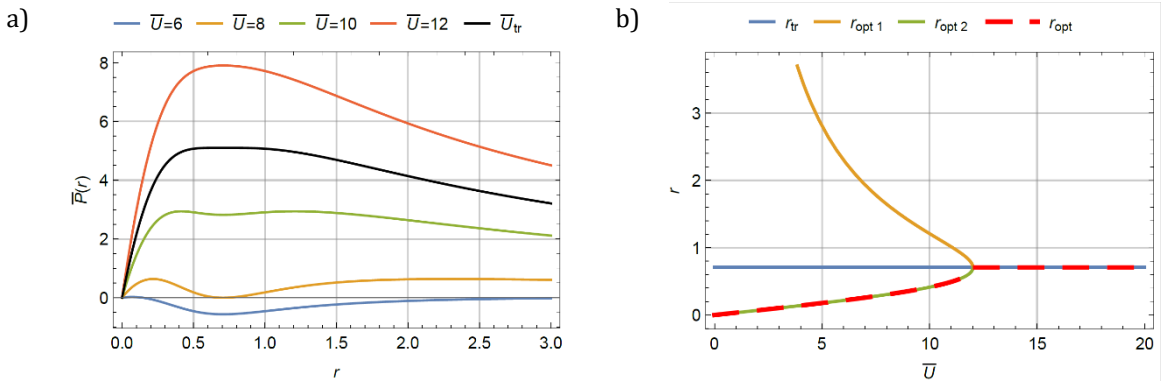

Fig. 3. a) Variation of electrical power $\bar{P}$ with electrical resistance r for the linear model; b) Optimal value of electrical resistance r_{opt} vs flow velocity $\bar{U}$ for the linear model.

According to Figure 3a, for lower flow rates, two equivalent maxima can be indicated. Along with flow velocity tending to a certain threshold value $\bar{U}_{tr} = 2\frac{\zeta+(\sqrt{1+\kappa}-1)}{a_1\bar{\rho}}$, the resistance values corresponding to these points are tending to a value r_{tr}, given by the expression:

$$r_{tr} = \frac{1}{\sqrt{1+\kappa}}, \tag{29}$$

which in Figure 3a is represented as the local minimum. When it is reached, these characteristic points disappear, as a result of which the value of r_{tr} becomes the global maximum, thus for $\bar{U} \geq \bar{U}_{tr}$ the optimal value of dimensionless resistance $r_{opt} = r_{tr}$. For $\bar{U} < \bar{U}_{tr}$ functions r_{opt1} or r_{opt2} can be adopted as r_{opt}, however due to the finite domain of the r_{opt2} it is a better choice. The optimal value of r for the full $\bar{U}$ spectrum is therefore a function:

$$r_{opt} = \begin{cases} r_{opt2}(\bar{U}), & \bar{U} < \bar{U}_{tr} \\ r_{tr}(\bar{U}), & \bar{U} \geq \bar{U}_{tr} \end{cases}. \tag{30}$$

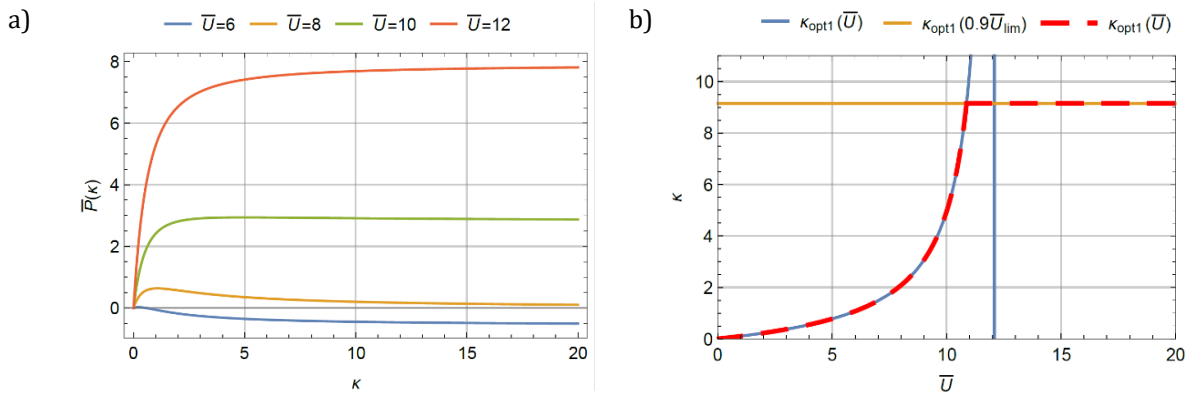

Fig. 4. a) Variation of electrical power $\bar{P}$ with electromechanical coupling κ for the linear model; b) Optimal value of electrical resistance κ_{opt} vs flow velocity $\bar{U}$.

Adopting such value of r_{opt} also leads to the fact that $\lim_{r\to 0} \bar{U}_{cr} = 0$, therefore, the device will perform work for infinitesimal low flow velocities. The strictly optimal value of the dimensionless electromechanical coupling κ_{opt1} can only be determined for $\bar{U} \in < 0; \bar{U}_{lim})$, where:

$$\bar{U}_{lim} = \frac{2(r\zeta+1)}{a_1\bar{\rho}r}. \tag{31}$$

Because $\lim_{\bar{U}\to\bar{U}_{lim}} \kappa_{opt1} = \infty$. Therefore, parameter κ_{opt} was adopted as a function of the form:

$$\kappa_{opt} = \begin{cases} \kappa_{opt1}(\bar{U}), & \bar{U} < 0.9\bar{U}_{lim} \\ \kappa_{opt1}(0.9\bar{U}_{lim}), & \bar{U} \geq 0.9\bar{U}_{lim} \end{cases}. \tag{32}$$

3.2. Nonlinear system

Physical model of the device with stiffness described by eq. (33) is presented in Figure 5a also in this device variant there are no characteristic stiffness parameters, thus the optimization comes down to the selection of proper r and κ functions.

$$\frac{\partial \Psi}{\partial w(\tau)} = w^3(\tau). \tag{33}$$

Considering the nature of nonlinear systems, it can be expected that the amplitude and frequency of the vibrations of the system will depend on each other. By utilizing eqs. (21, 22), these relations were (34, 35):

$$A_w = 2\sqrt{\frac{r\bar{U} - a_1\bar{\rho}\bar{U}^2 + 2\bar{U}\zeta - a_1\bar{\rho}r^2\bar{U}^2\Omega^2 + 2r^2\bar{U}\zeta\Omega^2}{3a_3\bar{\rho}\Omega^2(1 + r^2\Omega^2)}}, \tag{34}$$

$$\Omega = \sqrt{\frac{1}{2}\left(\frac{3}{4}{A_w}^2 - \frac{1}{r^2} + \kappa + \frac{\sqrt{48r^2{A_w}^2 + \left(4 - 3r^2{A_w}^2 - 4r^2\kappa\right)^2}}{4r^2}\right)}. \tag{35}$$

Through the solution of the system composed of these two equations, one can get the explicit expression for the vibration amplitude necessary to calculate the voltage and power. Figure 5b compares the obtained analytical solution with the numerical one. One can observe a clear, but considering the purpose of the work, the neglectable difference in critical speeds for solutions obtained by both methods. Besides, there is, more pronounced than in the linear system, shifting of solutions, progressing with the increasing flow velocity. However, compliance was considered sufficient.

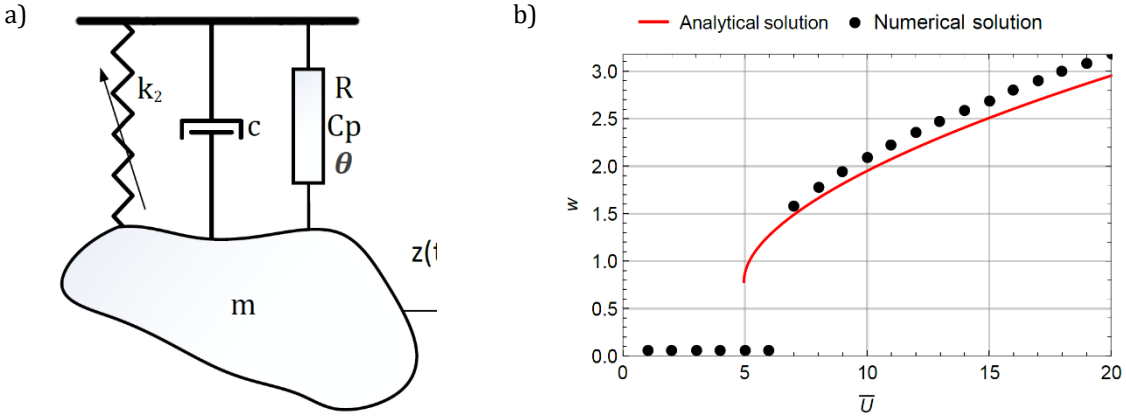

Fig. 5. a) Model of the nonlinear device; b) Variation of vibration amplitude w with flow velocity $\bar{U}$ for the nonlinear model.

Figure 6a and Figure 6b show the functions $\bar{P}(r)$ and $\bar{P}(\kappa)$ respectively for different flow velocities. As can be seen, these functions are similar to those of a linear system. Similarly as there, the $\bar{U}_{tr}$ and $\bar{U}_{lim}$ velocities can be observed forcing the discontinuity of optimal values of the parameter. The most significant difference concerns $\bar{P}(r)$ function, where – in contrast to the linear system – the value of r_{tr} depends on the flow velocity.

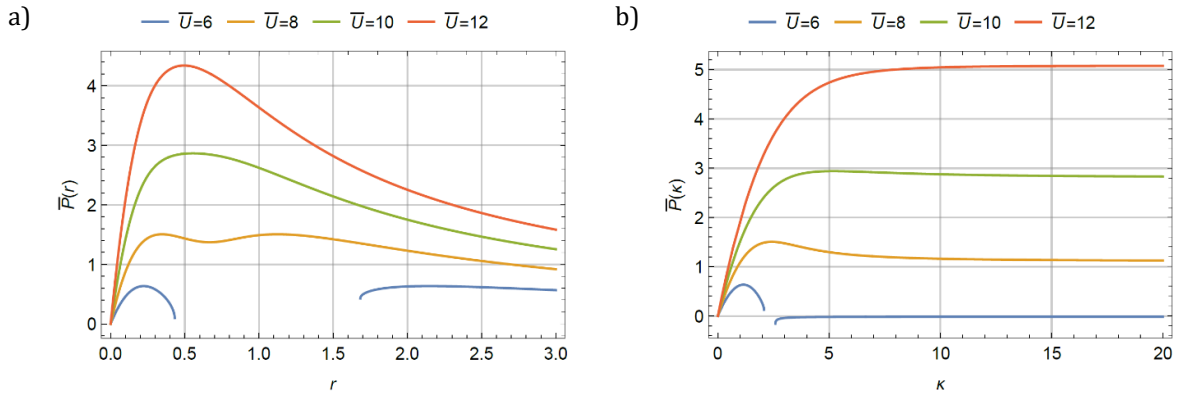

Fig. 6. a) Variation of electrical power $\bar{P}$ with electrical resistance r for the nonlinear model; b) Variation of electrical power $\bar{P}$ with electromechanical coupling κ for nonlinear model.

3.3. The system with combined stiffness

By combined stiffness model is meant a system in which the elastic force has two elements: linear and non-linear, in this case, proportional to the third power of deflection from the equilibrium position. Its physical model is shown in Figure 7a. The dimensionless elastic force takes the form:

$$\frac{\partial \Psi}{\partial w(\tau)} = w(\tau) + k_N\, w^3(\tau), \tag{36}$$

where: $k_N = \frac{k_2\, h^2}{m\, {\omega_n}^2}$ – dimensionless nonlinear stiffness coefficient. It is a structural parameter, characteristic for the system, so it is advisable to determine its impact on the device power. The expression for the vibration amplitude of the system was obtained by solving the system of equations (19, 20). A comparison of analytical and numerical solutions (Figure 7b) does not reveal significant differences. Functions $\bar{P}(r)$ (Figure 8a) and $\bar{P}(\kappa)$ (Figure 8b) exhibit the same characteristics as analogous functions for a nonlinear system. However, the most noteworthy is the function $\bar{P}(k_N)$. As shown in Figure 8c, the optimal value of k_N, independent of the flow velocity, is $k_N = 0$, which is synonymous with eliminating nonlinearity in the system and thus reducing it to the already analyzed linear system. This proves the fact that the application of the system with a combined stiffness is unfounded.

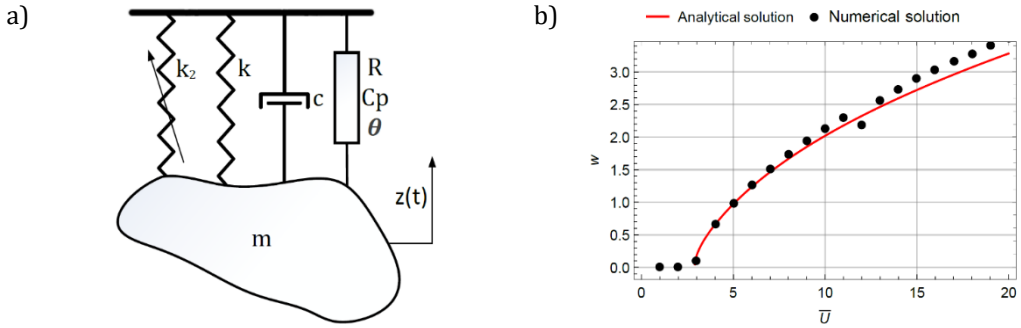

Fig. 7. a) Physical model of the device with combined stiffness; b) Variation of vibration amplitude w with flow velocity $\overline{U}$ for the model with combined stiffness.

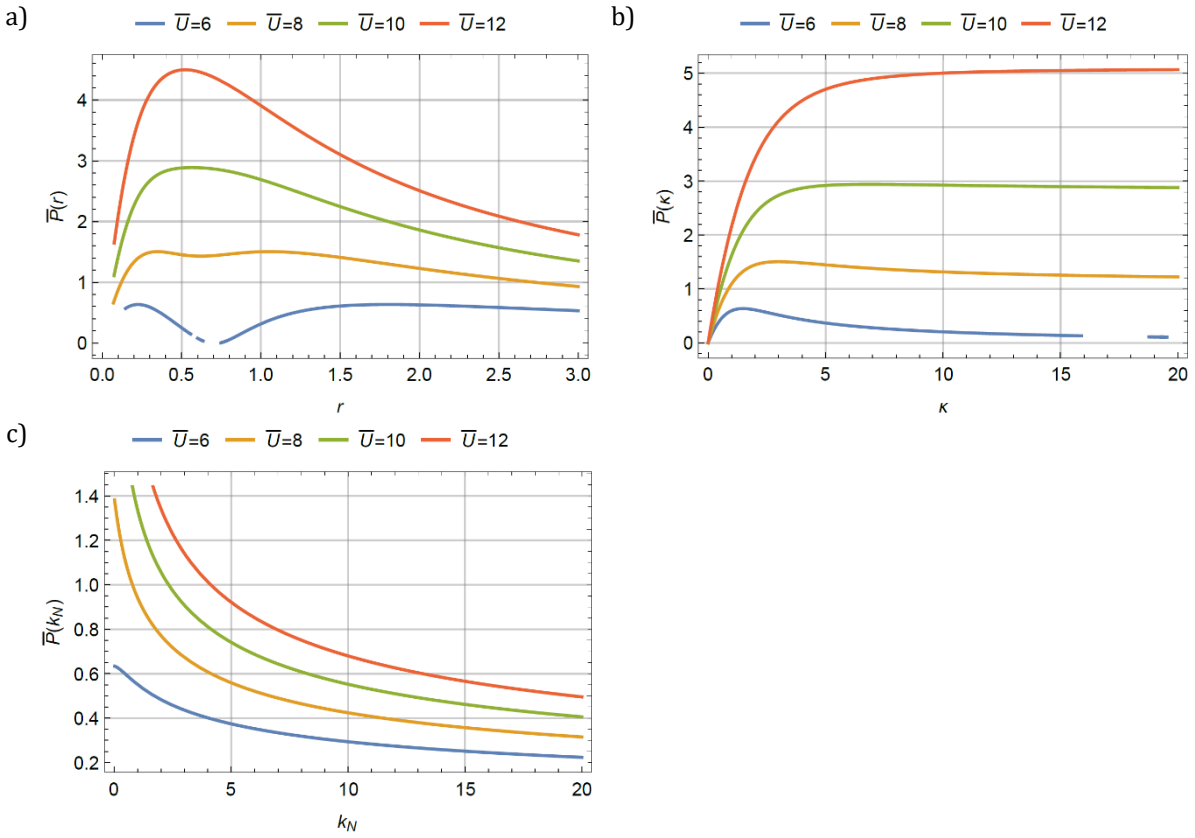

Fig. 8. a) Variation of electrical power $\overline{P}$ with electrical resistance $\overline{U}$ for the model with combined stiffness; b) Variation of electrical power $\overline{P}$ with electromechanical coupling κ for the model with combined stiffness; c) Variation of electrical power $\overline{P}$ with electrical resistance k_N for the model with combined stiffness.

3.4. Bistable system

A bistable system is one that has two equilibrium positions. This effect was achieved by supporting the resonator on two springs, whose orientation is described by two parameters: L_x and L_z (Figure 9a). The dimensionless elasticity force in the system is given by the expression:

$$\frac{\partial \Psi}{\partial w(\tau)} = w(\tau)\left(1 - \frac{\sqrt{\overline{L_x}^2 + \overline{L_y}^2}}{\sqrt{\overline{L_x}^2 + w^2(\tau)}}\right), \tag{37}$$

where: $\overline{L_x} = \frac{L_x}{h}$ and $\overline{L_z} = \frac{L_z}{h}$ are the dimensionless distance between the spring joints in X and Z direction respectively. Even though the system two fixed points, adopting the solution form of (12, 13) ensures sufficient accuracy (Figure 9b).

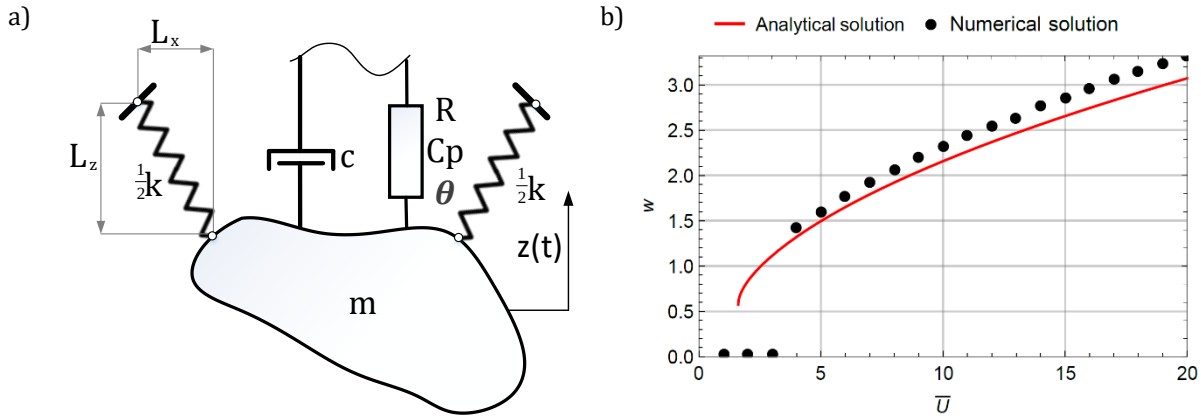

Fig. 9. a) Model of the bistable device; b) Variation of vibration amplitude w with flow velocity $\overline{U}$ for a bistable model.

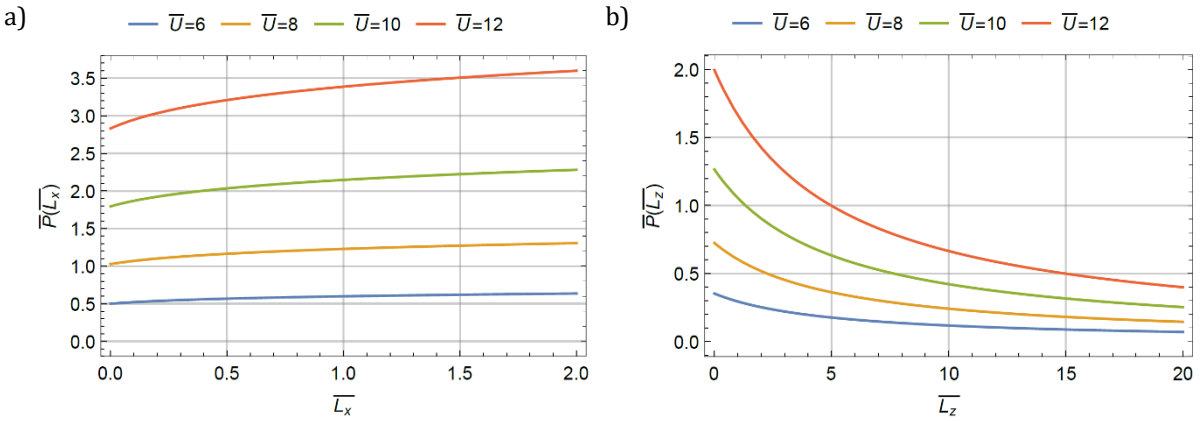

Fig. 10. a) Variation of electrical power $\overline{P}$ with electrical resistance $\overline{U}$ for bistable system; b) Variation of electrical power $\overline{P}$ with electromechanical coupling κ for the bistable system.

Analysis of the function $\overline{P}(\overline{L_x})$ (Figure 10a) and $\overline{P}(\overline{L_z})$ (Figure 10b) indicates that the optimal values of the parameters $\overline{L_x}$ and $\overline{L_z}$ are infinity and zero, respectively. Compliance with any of these conditions will lead to the disappearance of bistability: in the case when $\overline{L_x} = 0$, the system will become linear, while for $\overline{L_z} = \infty$, springs will be arranged along the X-direction. Therefore, there are a strong base to reject the thesis that the bistability of energy harvester promotes its performance. However, the indicated special case can be analyzed for which the springs are arranged in the transverse direction, thus $\overline{L_x} = \overline{L}$ and $\overline{L_z} = 0$.
The function of the dimensionless restoring force in this case is:

$$\frac{\partial \Psi}{\partial w(\tau)} = w(\tau)\left(1 - \frac{\overline{L}}{\sqrt{\overline{L}^2 + w^2(\tau)}}\right), \tag{38}$$

where $\overline{L} = \frac{L}{h}$ stands for the dimensionless length of the spring. Figure 11 show graphs of $\overline{P}(r)$, $\overline{P}(\kappa)$ and $\overline{P}(\overline{L})$ dependencies, respectively. The first two exhibit the same features as analogous functions obtained for other nonlinear models. Analysis of the function $\overline{P}(\overline{L})$ shows that there is a certain, dependent on the flow velocity, optimal value of the parameter $\overline{L}$.

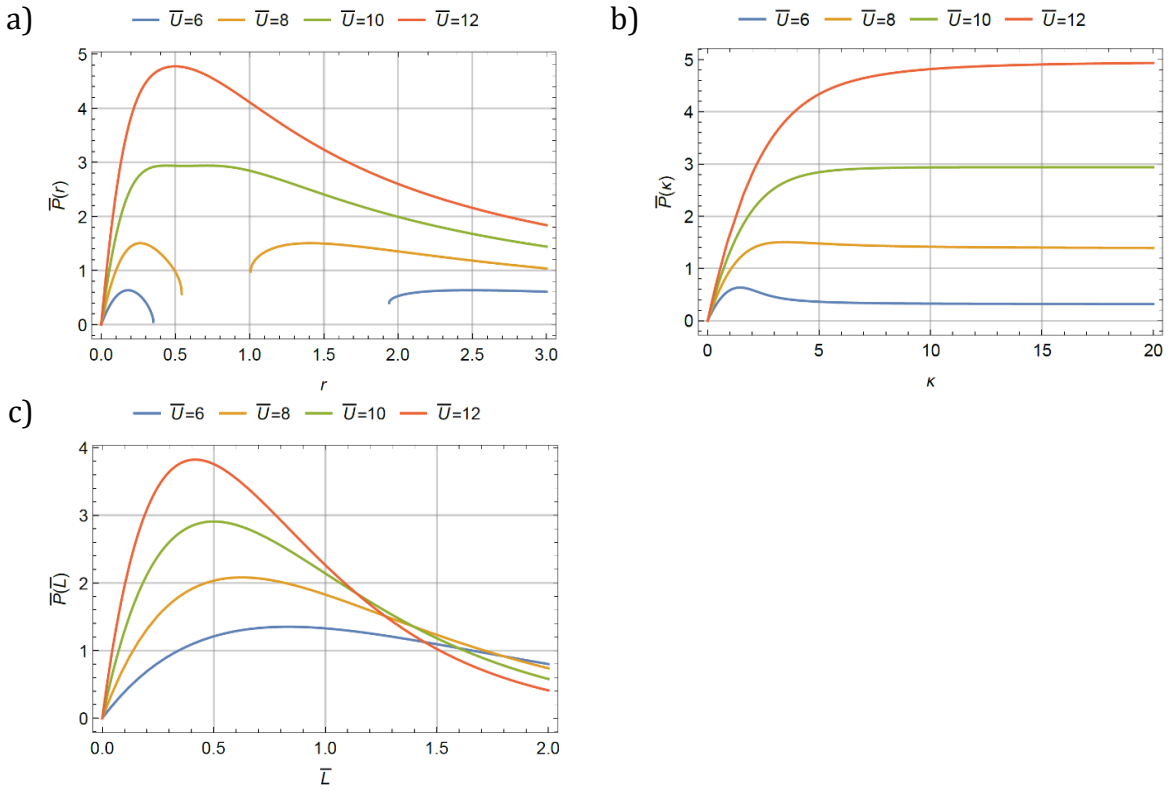

Fig. 11. a) Variation of electrical power $\bar{P}$ with electromechanical coupling κ for the transverse model; b) Variation of electrical power $\bar{P}$ with spring length $\bar{L}$ for transverse model; c) Variation of vibration amplitude w with flow velocity $\bar{U}$ for the transverse system.

4. Conclusions and discussion

The study of each system was preceded by deriving dimensionless analytical equations describing the power generated by various device variants. For this purpose, the Galerkin method was used while adopting a simplifying assumption about the sinusoidal motion of the device. The accuracy of this assumption was tested each time by comparing the obtained solution with a numerical one.

By analyzing the obtained solutions, the impact of individual model parameters on the generated power was examined. The parameters that are affecting every model, i.e. dimensionless electrical resistance r and electromechanical coupling κ, turned out to be similar for each device variant. The only significant difference is the fact that in the case of a linear system above a certain threshold flow velocity $\bar{U}_{tr}$, the optimal value of the dimensionless electrical resistance r takes a constant value. In other cases, the optimal value of both parameters changes varies with the flow velocity in its full domain.

Additional parameters related to the description of the potential energy of the system occurred in two non-linear models: combined stiffness and bistable. The analysis of their impact on power showed the unfounded use of devices of this design. In the case of a device with combined stiffness, the optimization led to the disappearance of nonlinearity, while for a bistable device it was associated with the disappearance of the nonlinearity or its maintenance while the loss of bistability. The last, special case was treated as the last variant and together with the other variants, it was optimized.

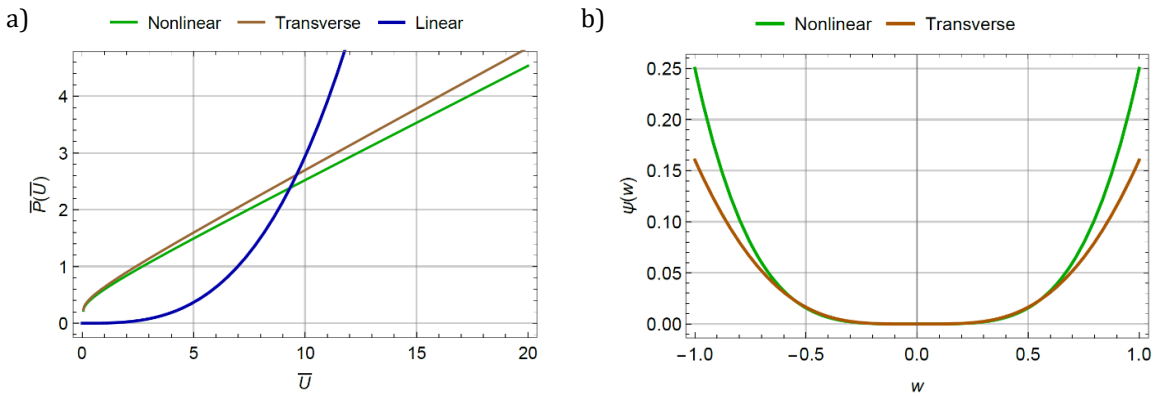

Fig. 12. a) Variation of electrical power $\bar{P}$ with electromechanical coupling $\bar{U}$ for different device variants; b) Dimensionless potential energy $\Psi(w)$ vs w for the nonlinear and transverse model.

Figure 12a shows the $\bar{P}(\bar{U})$ functions for the various device variants with optimized parameters. It points out that both nonlinear systems are more efficient than linear only at low flow velocities. It should be emphasized that due to the nature of these functions, this effect will remain also for a non-optimal set of parameters – provided that the critical velocity $\bar{U}_{cr}$ of nonlinear systems is not high enough that the functions will not intersect. The great similarity in the efficiency of both nonlinear systems caused by the fact that, despite the significant difference in the models of these devices, their potential energy functions $\Psi(w)$ are almost identical (Figure 13b). A small, nearly 7% difference in favor of the transverse system should be seen in the fact that it is described by one additional parameter (spring length $\bar{L}$), which allows for a more precise adjustment of the restoring force function.

Acknowledgments

This paper was financially supported by the grant: 0612/SBAD/3567.

References

1. J.P. Den Hartog. Mechanical Vibrations, fourth ed. McGraw-Hill, New York, USA, 1956.
2. M. Novak. Aeroelastic galloping of prismatic bodies. Journal of the Engineering Mechanics Division, 96:115–142, 1969.
3. Y. Ng, S. C. Luo, Y. T. Chew. On using high-order polynomial curve fits in the quasi-steady theory for square-cylinder galloping. Journal of Fluid and Structures, 20(1):141–146, 2005.
4. A. Abdelkefi, M. R. Hajj. A. Nayfeh. Power harvesting from transverse galloping of square cylinder. Nonlinear Dynamics 70:1355–1363, 2012.
5. S. Boisseau, G. Despesse, B. Ahmed Seddik. Electrostatic Conversion for Vibration Energy Harvesting. Small-Scale Energy Harvesting, Intech, 2012. doi: 10.5772/51360.
6. A. Kumar, S. S. Balpande, S. C. Anjankar. Electromagnetic Energy Harvester for Low Frequency Vibrations Using MEMS. Procedia Computer Science, 79:785-792, 2016.
7. P. Carneiro, M.P.S. dos Santos, A. Rodrigues, J.A. Ferreira, J.A. Simões, A.T. Marques, A.L. Kholkin. Electromagnetic energy harvesting using magnetic levitation architectures: A review. Appl. Energy, 260:114191, 2020.
8. B.G. Baraskar, T.C. Darvade, R.C. Kambale, J. Ryu, V. Annapureddy. Harvesting stray magnetic field for powering wireless sensors. Ferroelectric Materials for Energy Harvesting and Storage. Elsevier, Amsterdam, The Netherlands, 249–278, 2021.
9. R. Saibal. Electromechanical—MEMS Vibrational Energy Harvesting. Integrated ICT Hardware & Systems. Tyndall National Institute. Dublin, Ireland, 2021.
10. A. Abdelkefi, A. Nayfeh, M. R. Hajj. Modeling and analysis of piezoaeroelastic energy harvesters, Nonlinear Dynamics, 67(2):925-939, 2011.

11. C. Covaci, A. Gontean, Piezoelectric Energy Harvesting Solutions: A Review. Sensors, 20(12):3512, 2020.
12. C. Howells. Piezoelectric energy harvesting. Energy Conversion and Management, 50:1847-1850, 2009.
13. C. De Marqui, A. Erturk, D. J. Inman. An electromechanical finite element model for piezoelectric energy harvester plates. Journal of Sound and Vibration, 327:9-25, 2019.
14. G. Alonso, J. Meseguer, A. Sanz-Andres, E. Valero. On the galloping instability of two-dimensional bodies having elliptical cross-sections. Journal of Wind Engineering and Industrial Aerodynamics, 98:438-448, 2010.
15. N. J. Nikitas, H. G. Macdonald. Misconceptions and Generalizations of the Den Hartog Galloping Criterion. Journal of Engineering Mechanics, 140(4), 2014.
16. J. Meseguer, A. Sanz-Andres, G. Alonso. Determination of Maximum Mechanical Energy Efficiency in Energy Galloping Systems. Journal of Engineering Mechanics, 141:1355–1363, 2015.
17. J. Kluger, F. C. Moon, E. Rand. Shape optimization of a blunt body Vibro-wind galloping oscillator. Journal of Fluids and Structures, 40:185-200, 2013.
18. A. Barrero-Gil, G. Alonso, and A. Sanz-Andrés. Energy harvesting from transverse galloping. Journal of Sound and Vibration, 329(14):2873– 2883, 2010.
19. S. Jo, W. Sun, C. Son, Galloping-based energy harvester considering enclosure effect. AIP Adv, 8(9), 2018.
20. Y. Wu, D. Li, J. Xiang. Dimensionless modeling and nonlinear analysis of a coupled pitch–plunge–leadlag airfoil-based piezoaeroelastic energy harvesting system. Nonlinear Dynamics, 92(2):153–167, 2018.
21. M. Hwang, A. Arrieta. Input-Independent Energy Harvesting in Bistable Lattices from Transition Waves. Scientific Report, 8(1), 2018.
22. R. Vasconcellos, A. Abdelkefi. Nonlinear dynamical analysis of an aeroelastic system with multi-segmented moment in the pitch degree-of-freedom. Communications in Nonlinear Science and Numerical Simulation, 20(1):324-334, 2015.
23. Y. Wu, D. Li, J. Xiang, A. Da Ronch. A modified airfoil-based piezoaeroelastic energy harvester with double plunge degrees of freedom. Theoretical and Applied Mechanics Letters, 6:244-247, 2016.
24. S. Liu, P. Li, Y. Yang. On the design of an electromagnetic aeroelastic energy harvester from nonlinear flutter. Meccanica, 53:2807–2831, 2018.
25. H. Elahi, M. Eugeni, L. Lampani. Modeling and Design of a Piezoelectric Nonlinear Aeroelastic Energy Harvester. Integrated Ferroelectrics, 211(1):132-151, 2020.
26. J. Wang, L. Geng, S. Zhou. Design, modeling and experiments of broadband tristable galloping piezoelectric energy harvester. Acta Mechanica Sinica,36:592–605, 2020.